

Cable Loop Calibration System for Jiangmen Underground Neutrino Observatory

Yuanyuan Zhang^a, Jiaqi Hui^a, Jianglai Liu^{a,b}, Mengjiao Xiao^{c,d,*}, Tao Zhang^{a,**}, Feiyang Zhang^a, Yue Meng^a, Donglian Xu^{b,a}, Ziping Ye^b

^a*School of Physics and Astronomy, Shanghai Jiao Tong University, Shanghai Key Laboratory for Particle Physics and Cosmology, Shanghai 200240, China*

^b*Tsung-Dao Lee Institute, Shanghai Jiao Tong University, Shanghai, 200240, China*

^c*Department of Physics, University of Maryland, College Park, Maryland 20742, USA*

^d*Center of High Energy Physics, Peking University, Beijing 100871, China*

Abstract

A cable loop source calibration system is developed for the Jiangmen Underground Neutrino Observatory, a 20 kton spherical liquid scintillator neutrino experiment. This system is capable of deploying radioactive sources into different positions of the detector in a vertical plane with a few-cm position accuracy. The design and the performance of the prototype are reported in this paper.

Keywords: JUNO, Calibration system, Cable loop system, CLS

1. Introduction

The Jiangmen Underground Neutrino Observatory (JUNO) is a 20 kton multi-purpose liquid scintillator (LS) detector, located 53 km from the Yangjiang and Taishan nuclear power plants in south China [1]. Its physics goal is to determine the neutrino mass ordering (MO) via the measurement of electron anti-neutrino energy spectrum with unprecedented precision [2, 3, 4, 5] and study the neutrino oscillation and the astrophysical neutrinos [1]. The LS of the central detector (CD) is confined by an acrylic sphere with an inner diameter of 35.7 m, outside of which there is an ultra-pure water shielding. Approximately 17000 20-inch photomultiplier tubes (PMTs) and 25000 3-inch PMTs are located in the water viewing the LS.

*Corresponding author: mengjiaoxiao@gmail.com

**Corresponding author: tzhang@sjtu.edu.cn

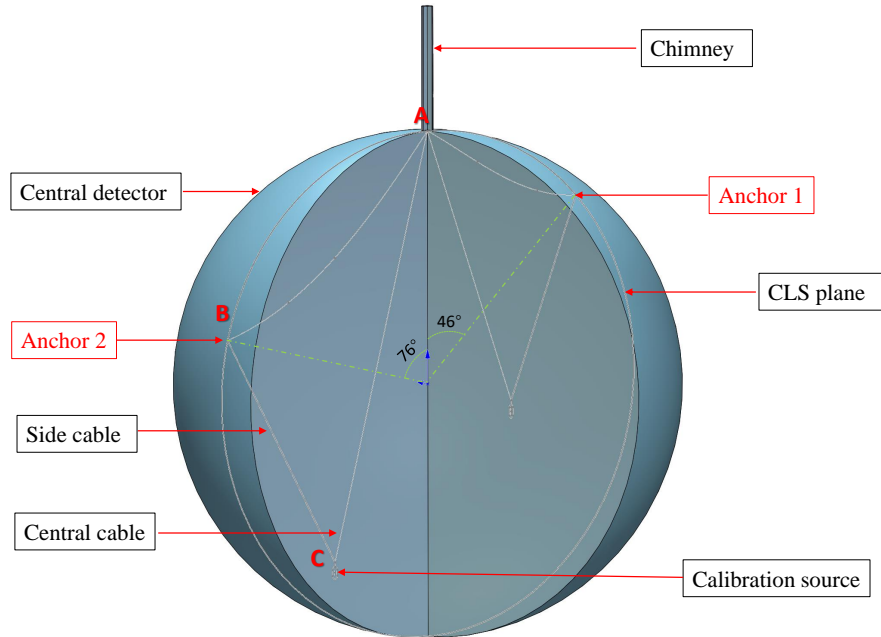


Figure 1: An illustration of the CLS. Two independent CLSs are envisioned to be installed in the JUNO detector to cover two half planes.

10 Detector non-uniformity needs to be calibrated to ensure the energy resolution required by the MO determination. Simulation studies have shown that we need to deploy radioactive sources to about 200 locations in a vertical plane of the detector and to make use of the azimuthal symmetry of the detector [6]. In this paper, we discuss the design and the prototype of an automatic system which can deliver the source to a wide range of positions via a cable loop, thus named the Cable Loop System or CLS. The design concept has been inspired by similar systems in SNO [7], KamLAND [8],
 15 and Borexino [9] experiments.

A sketch of the cable routing of the CLS is illustrated in Fig. 1. The cable loop is made up by a continuous cable which goes into the detector from the chimney, makes a complete loop via $A \rightarrow B \rightarrow C \rightarrow A$, then runs out of the detector. Point C is the attachment point of the source, on which
 20 an ultrasonic emitter is attached to allow accurate positioning. The segments connecting $A \rightarrow B \rightarrow C$ and $C \rightarrow A$ are referred to as the side cable and the central cable, respectively. The source can be delivered to a given position by adjusting the lengths of the side cable and the central cable.

The JUNO detector is mostly azimuthally symmetric by design, but the response function in radial and polar angle direction is complex [6]. Therefore, we have to access the off-center locations in a vertical half plane at the very least. In JUNO we design two independent CLSs, each covering a half-plane, to reach a larger accessible area and to facilitate the cross-check of the azimuthal symmetry.

The rest of this paper is organized as follows. In Section 2, we describe the design and prototype of the CLS, followed by a discussion of the motion sequence in Section 3. The performance of the prototype and the projected accessible area for the full-size detector are discussed in Section 4, followed by a summary in Section 5.

2. System design and prototype construction

2.1. Overview of the CLS in the calibration house

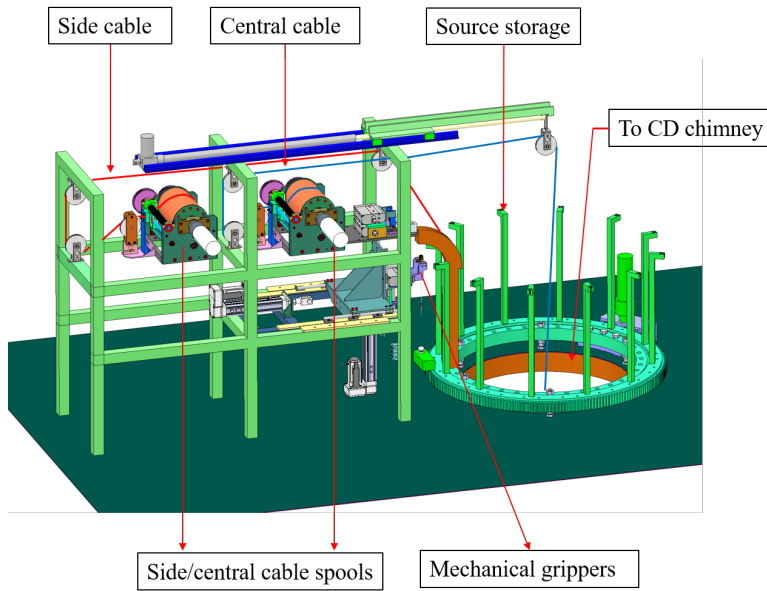


Figure 2: Side view of one CLS in the calibration house. See text for details.

The mechanical source delivery systems are located in the calibration house on top of the central detector, shown in Fig. 2. For each CLS, two spools are used to store the cables and to drive the central and side cables independently. Source assemblies are placed on the hanging frames on a

rotatable ring. A source can be attached to the CLS (point C in Fig. 1) and restored automatically by mechanical grippers or manually via the glove boxes.

2.2. Components of the CLS

40 2.2.1. Stainless steel cables

In the CLS, a large fraction of the cable will be permanently immersed in the liquid scintillator. The cable should satisfy four requirements: 1) be compatible with the LS in JUNO; 2) can supply power to the ultrasonic emitter [10]; 3) be flexible for source deployment and robust for more than 20 years of usage; 4) do not introduce significant radioactive background.

45 The selected cable is shown in Fig. 3. The Fluorinated ethylene propylene (FEP) jacket with 0.1 mm thickness is compatible with the LS, also with a low infiltration of the LS, which will bring little LS to the calibration house during the calibration. The cable has a 1.0 mm overall diameter with a turning radius of less than 5 mm. Its core consists of 7×7 strands of stainless steel wires, which makes that thermal expansion of the cable introduces a negligible effect. The average density
50 of the cable is around 3.565 g/cm^3 . The breaking strength is measured to be 60 kg. Each complete cable loop has a total length of 130 m, approximately. The radioactivity of the selected cable is reported elsewhere [11], leading to negligible contribution to the detector background.



Figure 3: A picture of the selected CLS cable. The top left corner shows the cross section of the cable.

2.2.2. Chimney collar and CLS anchor

In order to protect the joint between the chimney and the CD from the abrasion of the cables, a Polytetrafluoroethylene (PTFE) collar will be mounted on the underside of the joint, as shown in Fig. 4a. The PTFE has a small friction coefficient of 0.04, high photon reflectivity, low radioactivity, and is compatible with the LS. Two identical PTFE cable anchors with a spherical surface and a 50 mm turning radius (Fig. 4b) are designed to be installed on the inner surface of the acrylic sphere at polar angles 46° and 76° , optimized by simulations [6]. Despite that the frictions of these designs are larger than those using pulleys, the robustness is our top consideration for these components immersed permanently in the LS.

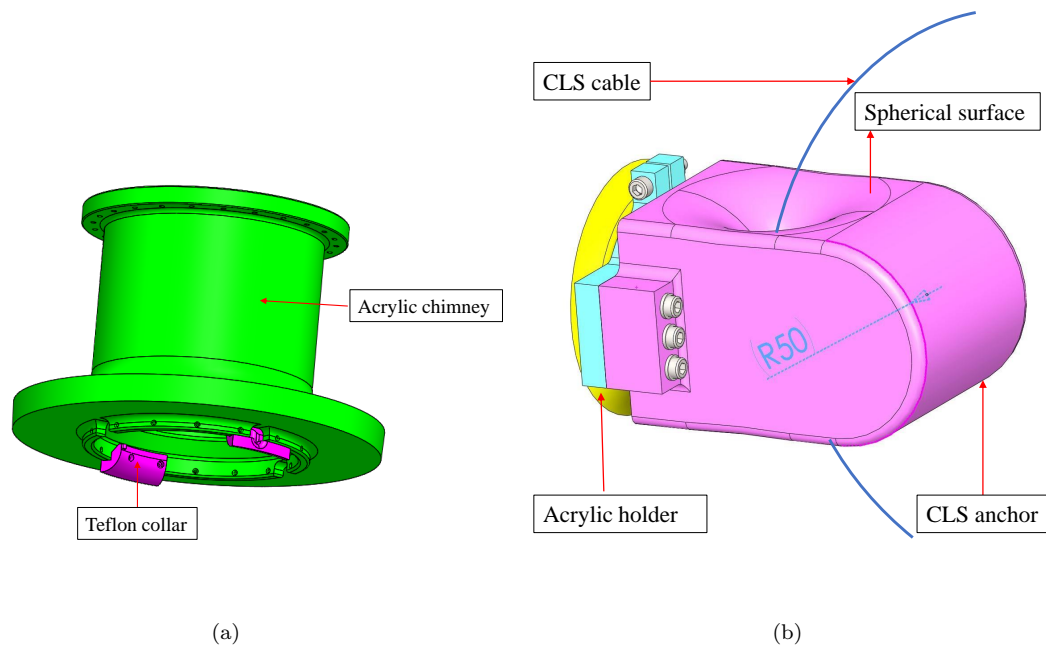


Figure 4: Design drawing of the chimney collars (a), mounted on the lowest segment of the CD chimney, and the CLS anchor with mounting fixture (b), the cable passes the anchor through a 1 mm hole.

2.2.3. Cable spools

Fig. 5 shows a picture of the cable spool system for one CLS. Two identical cable spools are designed, each driving the central/side cable. The spool is designed based on similar system used in the Daya Bay automated calibration system [12, 13]. The load cell with an accuracy of 0.025 N

is used to monitor the tension in the cables. A cable guide hole is designed to prevent de-groove of the cable. A servo motor (AKMH22E-CNT2GE5K [14]) is used to drive the spool, with its current monitored by the control software to avoid excessive torque. In order to reduce the friction and protect the stainless steel cables, all of the pulleys and spools are made out of the PTFE.

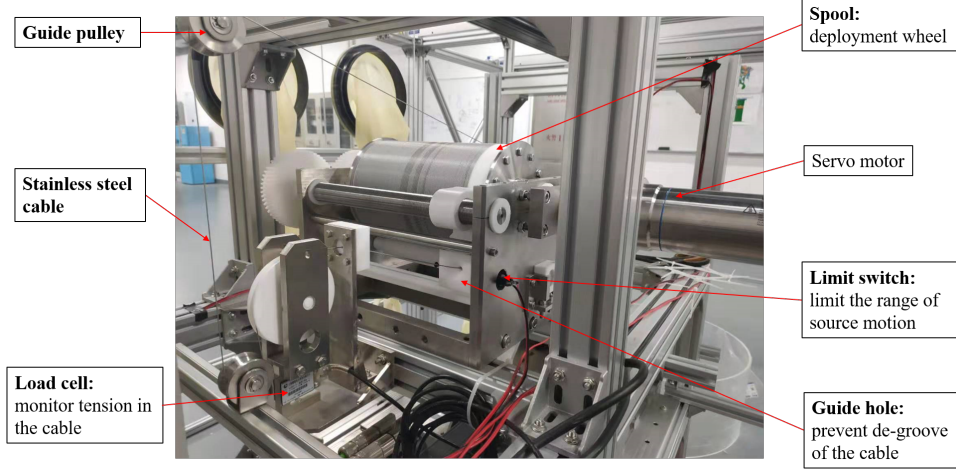


Figure 5: A picture of one cable spool of the CLS.

70 *2.2.4. Source assembly*

The basic design of a source assembly, from top to bottom, consists of a quick connector, a radioactive source container, and a bottom weight, inter-connected by about 20 cm of stainless steel cables, as shown in the Fig. 6a. The quick connector (male plug) can be inserted into the female receptacle attached to the CLS cable (Fig. 6b, also point “C” in Fig. 1). The ultrasonic
 75 emitter is attached to the female receptacle, with the CLS cable supplying electric driving power for the emitter. The bottom weight provides additional tension to keep the cables straight and to avoid cable slipping grooves. The bottom weight (~ 50 g) is made with normal nickel to allow potential rescue by a magnet. All pieces are made with PTFE enclosures to optimize photon reflectivity. The total weight of the source assembly (including the female receptacle and the ultrasonic emitter) is
 80 approximately 150 g.

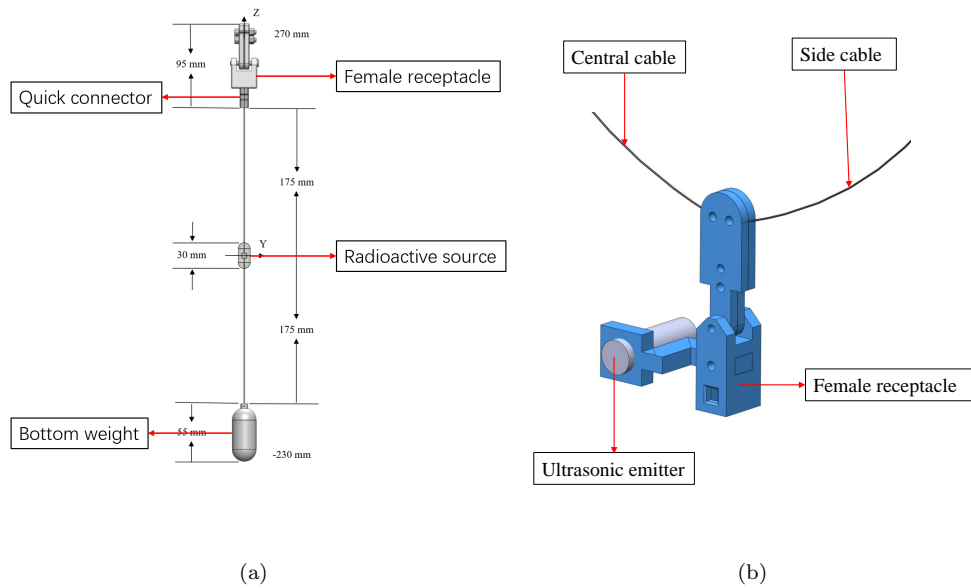


Figure 6: Design drawing of a source assembly (a); details of a female receptacle and the ultrasonic emitter (b).

2.3. Risks and mitigations

We have analyzed major risks associated with the failure of the CLS system, and incorporated mitigations into the system design. The considerations are summarized in Table 1. Each risk is counteracted with multiple mitigations.

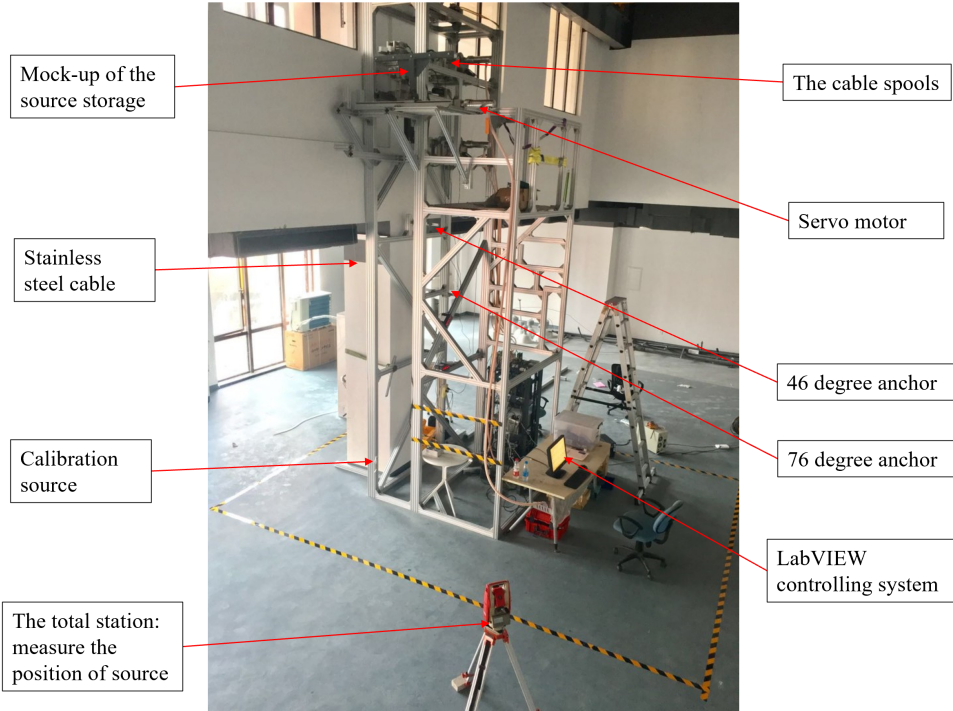


Figure 7: A picture of the CLS prototype in the lab.

As shown in Fig. 7, a prototype CLS is constructed in a lab with 8.5 m of overhead space, with both spools elevated by an aluminum frame. A LabVIEW control software is developed to control the spool motions. In this prototype, a mockup chimney collar and CLS anchors are installed to simulate realistic situations in JUNO. Due to limited vertical lab space, we varied the locations of PTFE anchors to simulate the CLS performance in 1/8 (4 m), 1/4 (8 m), 1/2 (18 m), and 1/1 (35.4 m) scale, but with different fractional coverage (see Fig. 8). The source positions are surveyed with a Total Station (KTS-442R4 [18]) with a few mm position accuracy.

3. Motion sequence

Realistic effects introduce difficulties in the CLS source position control. As illustrated in Fig. 9, the self weight of the cable and the friction from the anchor to the side cable have a significant influence to the movement of the side cable. For example, in Case 1 and Case 2, the center cable

Table 1: The possible failure modes in the CLS

failure mode	risk	mitigations
cable loses tension	cable slips groove on the spool	1) set load cells lower limit to 0.2 N; 2) reverse motion to tighten the cable; 3) guide the cable back into grooves by hand via the glove box.
source assembly gets stuck (e.g. against the collar)	damage of the cable or source assembly	1) smooth surfaces in the design; 2) set the load cell upper limit to 10 N; 3) reverse motion then slowly back up.
load cell failure	cannot monitor the state of cables	1) use driving current in the servo motor as a tension indicator and set appropriate range; 2) visual feedbacks; 3) cover the chimney opening, access the calibration house, and replace the load cells when desired.
mechanical component failures	cannot move the source	1) pull central cable by hand through the glove box to rescue the source; 2) cover the chimney opening, access the calibration house, and replace failed components when desired.
power off during the calibration	calibration interruption	1) use UPS system to leave enough time to exit the calibration gracefully; 2) use industrial PLC system for the motion control [15], which keeps all data during power outage; 3) control software will save all data onto disk, which can be reloaded when restarted.
cable breakage	source drops into the CD	1) set upper limits in load cells and current limits in servo motors so cables never experience tensions larger than 10 N; 2) load test all cables/joints to 10 times of the maximum allowable tension; 3) were the source dropped into the CD, fish the source with the ROV [16] carrying a magnet.
failure of the anchor de-attached from the acrylic sphere	anchor drops into the CD	1) ensure the tension in the cable to be less than 20 N, corresponding to a conservative maximum local stress of 0.35 MPa (the long term allowable stress in acrylic is 5 MPa [17]); 2) attachment is fastened by bolt and nuts to avoid threads in the fixture

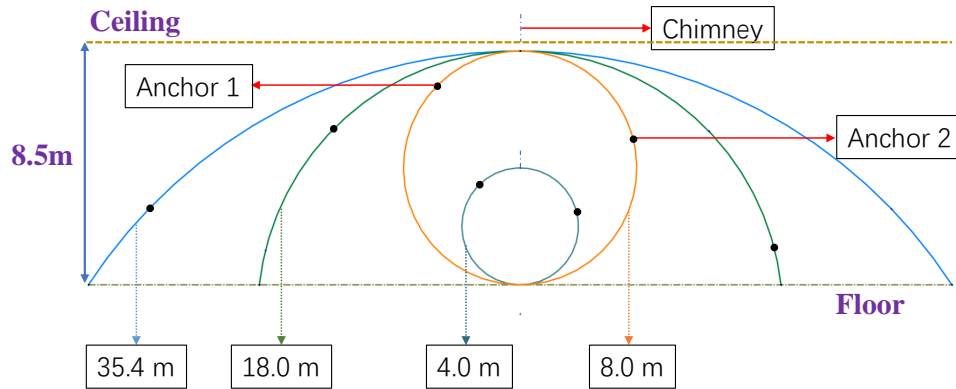


Figure 8: The mockup CLS planes constructed in the lab. Each circle represents a scaled version of the CD and corresponding CLS plane (see also Fig. 1), with the CLS anchor locations indicated as the black points.

stays the same and the side cable is actively pulled or passively released, respectively, reaching the same final cable length. The locations of the source are clearly different, and in Case 2 the section L' can be curved with poor repeatability (backlash). Therefore, in our motion sequence, the side cable should only be pulled or stay stationary. The center cable, on the other hand, can be released to reach the designated length as it is mostly free.

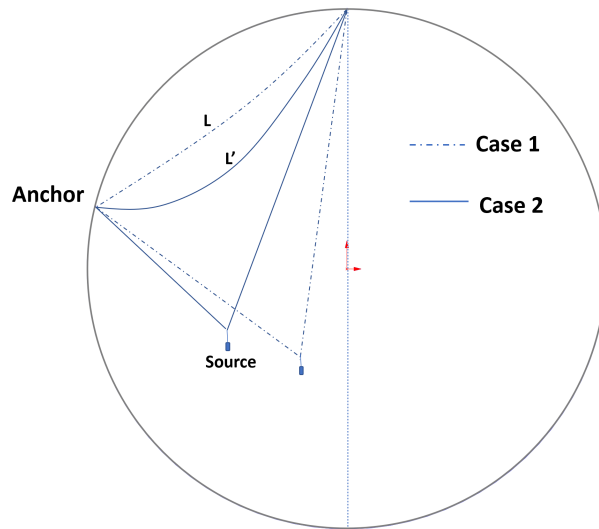


Figure 9: Illustration of the influence of the friction and cable self-weight to the CLS source position repeatability.

Following this guideline, the procedure of a source deployment sequence is illustrated in Fig. 10a. During the process, we study the tensions inside both cables using load cells close to the spools (Fig. 5). The results are shown in Fig. 10b. From point A to C1, the tension is kept to be 6(4) N in the central (side) cable, as both cables are mostly straight. From C1 to C2, there is a sharp decrease of the tensions due to sudden relaxations in both cables. The tension in the central cable decreases gently from C2 to C5 as the gravity of the source is taken up more and more by the side cable. However, the tension in the side load cell does not feel this until the source passes C4 when the friction at the anchor is overcome by the gravity of the source, leading to an increase in the load cell. Point C5 is the lower boundary of the motion, as the central cable loses its tension which triggers the interlock. We shall refer to this boundary as the CLS side boundary in the remainder of this paper.

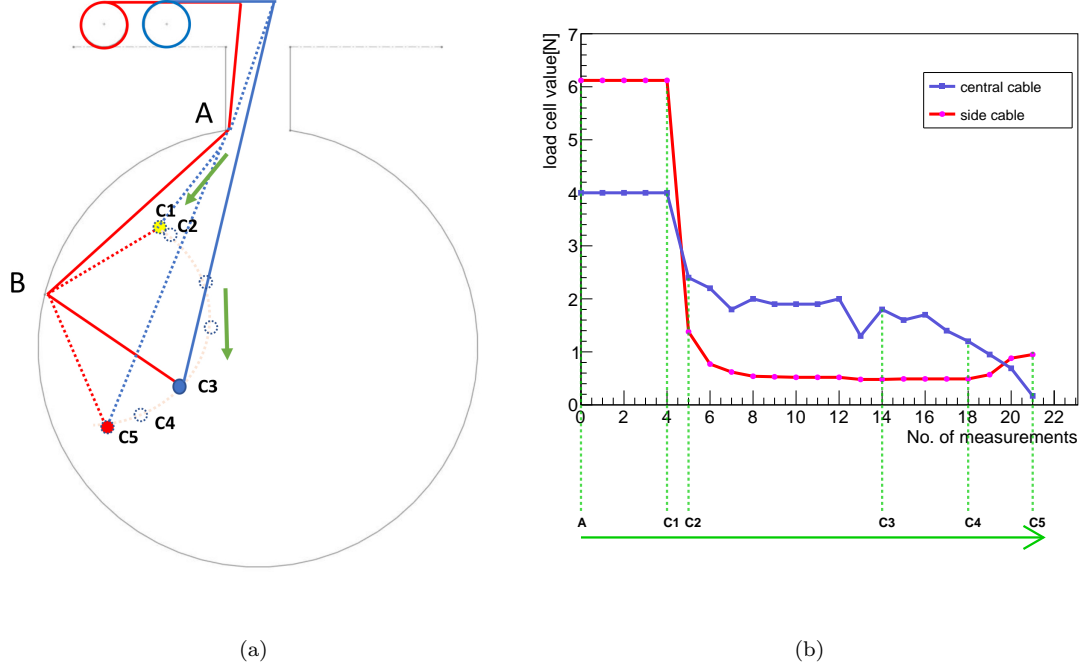


Figure 10: (a): illustration of the source motion from A to C1 to C5. Initially the central and side cables in the LS are mostly straight as we move the source through the chimney. When the source reaches the LS sphere, point C on Fig. 1 is at point A. To avoid the backlash in Fig. 9, it is sensible to move the source to C1 by pulling/releasing the side/central cables synchronously, then release the central cable to move the source to its designations (C2, C3, etc). (b): cable tension monitored by two load cells.

To go to the next (shorter) side cable length, we first move the source back from C5 to C1 by pulling the center cable, then do the synchronous motions to D1 (Fig. 11a). The motion along the arc from D1 to D2 etc. can be carried out similarly. The readings of load cell from C5 to D1 is shown in Fig. 11b. One observes increase of tension in the central cable as it is taking up more and more the gravity component. The tension in the side cable increases abruptly when the source moves from C2 to C1, as segments A-C1-B approach the straight line A-B. However, with limited tension in the cables, C1 can never touch A-B (the upper boundary of CLS). Such a procedure should be repeated in a single direction (reducing the side cable length) until the source gets close to B. To bring the source back to home, it will be moved along B-A, by the reverse synchronous motion (releasing the side cable and pulling the central cable).

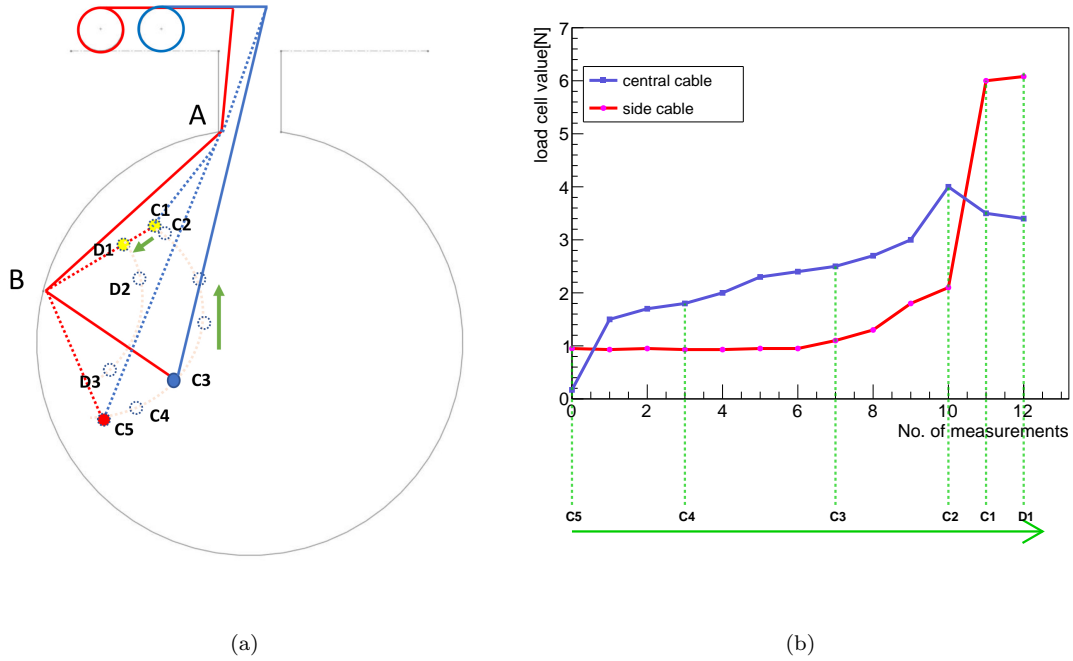


Figure 11: (a): moving from $C1$ to $D1$ by shortening the side cable, then along the $D1$ to $D3$ arc; (b): tensions in the cables.

In the entire process, the tension in the cables should be kept to be larger than 0.2 N to avoid cable slipping grooves on the spool and less than 10 N to protect the PTFE surfaces in direct contact with the cables.

4. System performance

Using the system shown in Fig. 8, realistic tests on the CLS prototype have been performed in circles with different diameters. The gravity of the source assembly is chosen to be 150 g, the effective weight after considering the LS buoyancy. To simulate the effect of the LS buoyancy to the 1 mm CLS cable (LS density 0.859 g/cm^3), the performance of 1 mm (350 g/100 m) and 0.8 mm (220 g/100 m) cables are compared. The friction is primarily due to CLS cable in touch with the chimney collar and the CLS anchor. In our tests, the collar and the anchor are made with the final design and surface treatment. Although infiltration of the LS to the PTFE surface would reduce the friction, the mock tests are performed with dry surfaces as a worst case.

135 *4.1. Accessible area*

Tensions in the cables are monitored during the tests. The effective coverage area is defined by three boundaries. The side boundary (tension in the central cable hitting the lower limit) and the upper boundary (tension in cables reaching the upper limit) have been discussed in Sec. 3. The central boundary, on the other hand, is due to the fact that non-zero tension in the side cable and
140 its self-weight always apply a horizontal force to bias the location of the source from the vertical line. These boundaries are shown in Fig. 12.

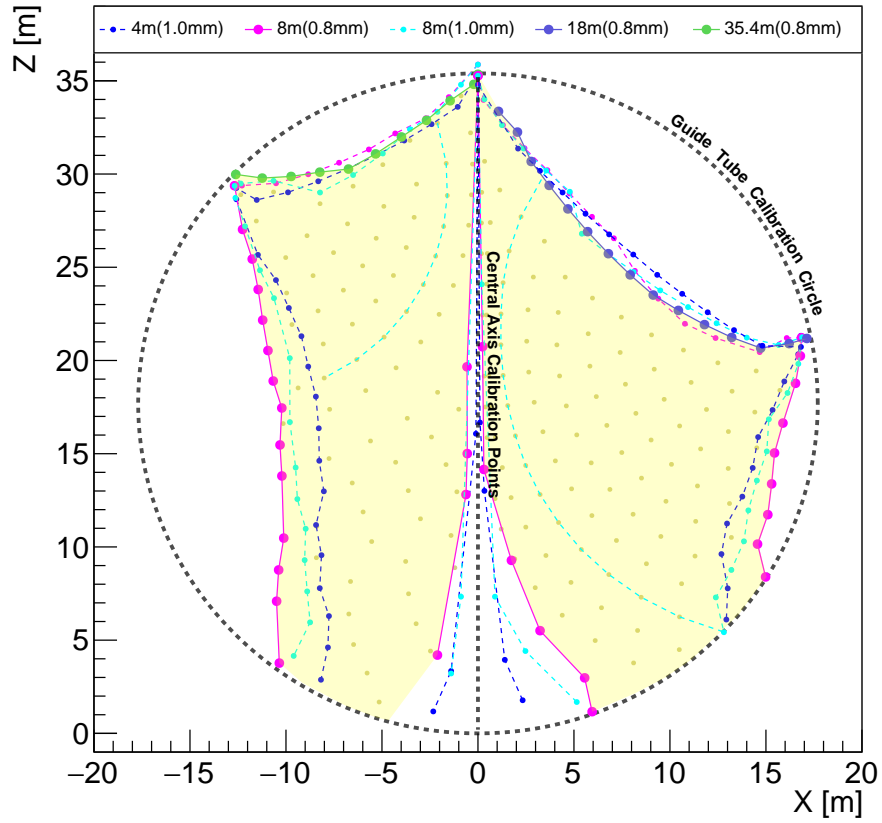


Figure 12: Results of the CLS tests. Each point in the figure represents a real location that was achieved in the tests, with different colors representing deployments in difference circles with a given cable (see legend). The green dashed circles indicate theoretical arcs when pulling the central cable with side cable stationary. The shaded area represents the predicted coverage in a full CD. JUNO also plans to have a central calibration unit covering the entire central axis(black-dashed line), and a guide tube covering a vertical circle of the sphere(black-dashed circle) [6], effectively increasing the positional coverage.

From the measurements, one observes that the accessible area 1) is mildly larger with the 0.8 mm cable, as expected, and 2) the upper, side, and central boundaries are going lower, outward, and less vertical when the diameter of the circle increases. We predict real CD coverage based on the 0.8 mm results with boundaries obtained in the largest possible circles in the test, shown as the shaded region in Fig. 12. In each half plane, the accessible area can reach 60% for the 46° anchor, and 66% for the 76° anchor. When the azimuthal symmetry is considered, the entire plane can be covered to 79%. The redundant coverage between the two half-planes also serves as a critical cross-check of the azimuthal-symmetry.

4.2. Repeatability

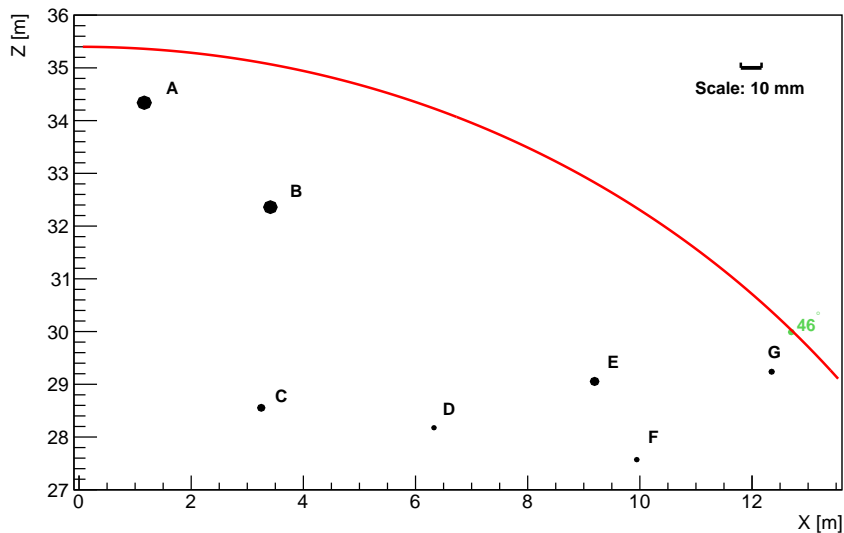


Figure 13: Position repeatability of seven points in the 35.4 m CLS test, with accessible locations limited by the lab setup. $Z = 35$ m represents the chimney-sphere joint. For each point, the diameter indicates the standard deviation from the position in the first deployment in the twelve repeated deployments. The typical values are shown in Table 2.

Ideally, calibration points are uniquely determined by the lengths of the cables ¹, but frictions, self-weight, etc are expected to introduce uncertainties. In the 35.4 m test, motion sequence of

¹Not by trigonometry, but by an empirical lookup table if an absolute calibration is carried out.

points	A	B	C	D	E	F	G
Standard deviation (mm)	6.8	6.5	3.5	2.2	4.1	2.1	2.5

Table 2: Standard deviation for seven points in the repeatability tests

A \rightarrow B \rightarrow C \rightarrow D \rightarrow E \rightarrow F \rightarrow G \rightarrow A \rightarrow ... (Fig. 13) are repeated twelve times and we measure the repeatability of the locations of the seven points. The results are shown in Fig. 13, with a worst
155 standard deviation of 6.8 mm. This indicates that once a motion sequence is fixed, the friction and backlash uncertainties are under good control. We note that in the real experiment, the absolute source position will be measured by the ultrasonic system. Nevertheless, the cable lengths can serve as an importance cross-check.

5. Summary

160 In this paper, we report the design and prototype performance of one of the key calibration systems, the cable loop system, of the JUNO experiment. The robustness of the system is tested rigorously with a complete function prototype at smaller scales in comparison to the real experiment. Based on the measurements, the CLS is capable to cover about 79% to a full plane of the central detector, with <10 mm positional repeatability. In combination with an extensive calibration
165 program discussed in Ref. [6], this CLS can satisfy the demanding requirements of the JUNO calibration.

6. Acknowledgement

This work is supported by the Strategic Priority Research Program of the Chinese Academy of Sciences, Grant No. XDA10010800, and the CAS Center for Excellence in Particle Physics
170 (CCEPP). We thank the support from the Office of Science and Technology, Shanghai Municipal Government (Grant No. 16DZ2260200), and the support from the Key Laboratory for Particle Physics, Astrophysics and Cosmology, Ministry of Education.

References

- [1] F. An, et al., Neutrino physics with JUNO, Journal of Physics G 43 (2016) 030401–030401.

- 175 [2] S. T. Petcov, M. Piai, The LMA MSW solution of the solar neutrino problem, inverted neutrino mass hierarchy and reactor neutrino experiments, *Physics Letters B* 533 (1) (2002) 94 – 106.
- [3] S. Choubey, S. T. Petcov, M. Piai, Precision neutrino oscillation physics with an intermediate baseline reactor neutrino experiment, *Phys. Rev. D* 68 (2003) 113006.
- [4] J. G. Learned, S. T. Dye, S. Pakvasa, et al., Determination of neutrino mass hierarchy and θ_{13} with a remote detector of reactor antineutrinos, *Physical Review D* 78 (2008) 071302.
- 180 [5] L. Zhan, Y. Wang, J. Cao, et al., Determination of the neutrino mass hierarchy at an intermediate baseline, *Physical Review D* 78 (2008) 111103.
- [6] F. Zhang, et al., Calibration strategy of the JUNO experiment, manuscript in preparation.
- [7] K. Boudjemline, et al., The calibration of the sudbury neutrino observatory using uniformly distributed radioactive sources, *Nuclear Instruments and Methods in Physics Research Section A: Accelerators, Spectrometers, Detectors and Associated Equipment* 620 (2) (2010) 171 – 181.
- 185 [8] B. E. Berger, et al., The KamLAND full-volume calibration system, *Journal of Instrumentation* 4 (04) (2009) P04017–P04017.
- [9] H. Back, et al., Borexino calibrations: hardware, methods, and results, *Journal of Instrumentation* 7 (10) (2012) P10018–P10018.
- 190 [10] G. Zhu, J. Liu, Q. Wang, et al., Ultrasonic positioning system for the calibration of central detector, *Nuclear Science and Techniques* 30 (001) (2019) 32–38.
- [11] F. Zhang, et al., The background of the JUNO calibration system, manuscript in preparation.
- [12] J. Liu, B. Cai, R. Carr, et al., Automated calibration system for a high-precision measurement of neutrino mixing angle θ_{13} with the daya bay antineutrino detectors, *Nuclear Instruments and Methods in Physics Research Section A: Accelerators, Spectrometers, Detectors and Associated Equipment* (2013).
- 195 [13] Y. Zhang, J. Liu, M. Xiao, et al., Laser calibration system in JUNO, *Journal of Instrumentation* 14 (01) (2019) P01009–P01009.

- 200 [14] AKMH22E-CNT2GE5K.
URL <https://www.kollmorgen.com/>
- [15] Y. Sun, A. Zhou, S. Xiao, Y. Wu, Q. Han, T. Zhu, Design of the PLC based switch control system for neutron beam line, Nuclear Techniques 38 (4) (2015).
- [16] K. Feng, D. Li, Y. Shi, et al., A novel remotely operated vehicle as the calibration system in JUNO, Journal of Instrumentation 13 (12) (2018) T12001–T12001.
205
- [17] J. Stachiw, Handbook of acrylics for submersibles, hyperbaric chambers and aquaria (12 2020).
- [18] KTS-442R4.
URL https://www.yiqi.com/product/detail_294094.html